AGU PUBLICATIONS

JGR

Journal of Geophysical Research: Oceans

RESEARCH ARTICLE

10.1002/2014JC010317

Key Points:
- This study addresses the remote forcing of the AMOC seasonal cycle
- Wind stress in subpolar basin forces AMOC changes in subtropics
- Topography and barotropic mode are important

Correspondence to:
J. Yang,
jyang@whoi.edu

Citation:
Yang, J. (2015), Local and remote wind stress forcing of the seasonal variability of the Atlantic Meridional Overturning Circulation (AMOC) transport at 26.5°N, *J. Geophys. Res. Oceans*, *120*, 2488–2503, doi:10.1002/2014JC010317.

Received 15 JUL 2014
Accepted 28 FEB 2015
Accepted article online 11 MAR 2015
Published online 2 APR 2015

Local and remote wind stress forcing of the seasonal variability of the Atlantic Meridional Overturning Circulation (AMOC) transport at 26.5°N

Jiayan Yang[1]

[1]Department of Physical Oceanography, Woods Hole Oceanographic Institution, Woods Hole, Massachusetts, USA

Abstract The transport of the Atlantic Meridional Overturning Circulation (AMOC) varies considerably on the seasonal time scale at 26.5°N, according to observations made at the RAPID-MOCHA array. Previous studies indicate that the local wind stress at 26.5°N, especially a large wind stress curl at the African coast, is the leading contributor to this seasonal variability. The purpose of the present study is to examine whether nonlocal wind stress forcing, i.e., remote forcing from latitudes away from 26.5°N, affects the seasonal AMOC variability at the RAPID-MOCHA array. Our tool is a two-layer and wind-driven model with a realistic topography and an observation-derived wind stress. The seasonal cycle of the modeled AMOC transport agrees well with RAPID-MOCHA observations while the amplitude is in the lower end of the observational range. In contrast to previous studies, the seasonal AMOC variability at 26.5°N is not primarily forced by the wind stress curl at the eastern boundary, but is a result of a basin-wide adjustment of ocean circulation to seasonal changes in wind stress. Both the amplitude and phase of the seasonal cycle at 26.5°N are strongly influenced by wind stress forcing from other latitudes, especially from the subpolar North Atlantic. The seasonal variability of the AMOC transport at 26.5°N is due to the seasonal redistribution of the water mass volume and is driven by both local and remote wind stress. Barotropic processes make significant contributions to the seasonal AMOC variability through topography-gyre interactions.

1. Introduction

The lower limb of the Atlantic Meridional Overturning Circulation (AMOC) is driven by the ventilation and export of the North Atlantic Deep Water (NADW)—a water mass that is formed by buoyancy-driven convection in the subpolar North Atlantic Ocean. Even though the mean AMOC state must be sustained by a stable source of NADW production, variations in the AMOC transport are forced by both buoyancy fluxes and surface wind stress. In fact, more studies increasingly point to the surface wind as the primary driver for seasonal-to-decadal variability of the AMOC transport in the subtropics [*Biastoch et al.*, 2008; *Kanzow et al.*, 2010; *Xu et al.*, 2014; *Zhao and Johns*, 2014; *Polo et al.*, 2014]. Numerical models that are forced only by wind stress are able to reproduce a seasonal cycle of AMOC that compares well with observations [*Zhao and Johns*, 2014]. Previous studies [*Kanzow et al.*, 2010; *Chidichimo et al.*, 2010], however, have mostly focused on local wind stress forcing. The role of remote forcing in seasonal AMOC variability has not been adequately studied previously.

Kanzow et al. [2010] and *Zhao and Johns* [2014] quantified the seasonal variability of the AMOC transport at 26.5°N by using observations from the UK-U.S. Rapid Climate Change—Meridional Overturning Circulation and Heat Flux Array (RAPID-MOCHA) array. The RAPID-MOCHA is the first boundary-to-boundary observational array [*Cunningham et al.*, 2007; *Johns et al.*, 2008, 2011; *Meinen et al.*, 2010, 2013]. *Kanzow et al.* [2010] used the first 4 years of data and showed that the AMOC transport strengthens in summer and fall, and weakens in late winter and early spring. *Zhao and Johns* [2014] extended this analysis with a longer record, and showed a similar pattern. As for the forcing mechanism, Kanzow et al. showed that the seasonal variability of the AMOC transport is mainly due to changes in the mid-ocean geostrophic transport between the Bahamas and Africa. They further demonstrated that baroclinic Rossby waves that are generated by wind stress curl along the eastern boundary at the Moroccan coast are primarily responsible for seasonal changes in the mid-ocean geostrophic transport.

An ocean circulation's response to a change in wind stress forcing is through both barotropic and baroclinic planetary Rossby waves [*Veronis and Stommel*, 1956] and the ocean's adjustment toward an equilibrium

state in a bounded ocean is through Kelvin and Rossby waves [*Anderson and Gill*, 1975]. The ocean does not fully equilibrate itself to a forcing without meridional propagation of either Kelvin or topographic Rossby waves [*Anderson and Gill*, 1975; *Kawase*, 1987; *Johnson and Marshall*, 2002]. So it is rather puzzling how baroclinic Rossby waves alone could dictate the seasonal cycle of the AMOC transport at 26.5°N. One has to wonder what roles do other types of waves play in the adjustment of the AMOC transport to seasonal wind stress forcing and where do those waves come from.

The main goal of this paper is to use a wind-driven model to investigate how surface wind stress forces seasonal variability of the AMOC transport at 26.5°N where a 10 year record is available. Specifically, we examine whether and how the seasonal AMOC cycle at this latitude is affected by wind stress changes in subpolar and tropical basins, a remote forcing mechanism that has been ignored in previous studies. We use a two-layer model to conduct our study. The paper is organized as follows. The model and the forcing fields will be introduced in the next section. This will be followed by discussions of model results and mechanisms in section 3. The study will be summarized in section 4.

2. Model and Forcing Field

The model used in this study is a two-layer, nonlinear, and primitive equation model that was used previously to study overflows from the Nordic Seas [*Yang and Pratt*, 2013, 2014]. It is similar to the model that was used by *Zhao and Johns* [2014] in their study of the seasonal variability of the AMOC transport. The version used in the present study is adiabatic, i.e., no diapycnal water mass flux between two layers. The model includes barotropic and the first baroclinic modes since both layers are active. The thickness of either layer is allowed to become zero (i.e., outcropping of the lower or grounding of the upper layer). The model is governed by the following equations:

$$\begin{aligned}
&\frac{d\vec{u}_1}{dt}+f\vec{k}\times\vec{u}_1=-g\nabla\eta-A\nabla^4\vec{u}_1-(1-H(h_2))\vec{F}_1+\frac{\vec{\tau}_{wind}}{\rho h_1}\\
&\frac{d\vec{u}_2}{dt}+f\vec{k}\times\vec{u}_2=-g\nabla\left(\eta+\frac{\Delta\rho}{\rho_2}\eta_2\right)-A\nabla^4\vec{u}_2-\vec{F}_2-(1-H(h_1))\frac{\vec{\tau}_{wind}}{\rho_2 h_2}\\
&\frac{\partial\eta}{\partial t}+\nabla\cdot\left(h_1\vec{u}_1+h_2\vec{u}_2\right)=0\\
&\frac{\partial h_2}{\partial t}+\nabla\cdot\left(h_2\vec{u}_2\right)=0
\end{aligned} \tag{1}$$

where (u_n, v_n) and h_n are velocity and layer thickness in the nth layer ($n = 1, 2$), η is the sea surface height, η_2 is the interface height anomaly, $A = 10^{12}$ m^4 s^{-1} is a biharmonic viscosity, $\vec{F}_n=\frac{\lambda|\vec{u}_n|\vec{u}_n}{h_n}$ is the bottom drag (where $\lambda = 0.005$ is a quadratic bottom drag coefficient), and $\Delta\rho = 1.5$ kg/m^3 is the water density difference between two layers. The lower layer is exposed to wind stress wherever it outcrops. Likewise, the bottom stress is applied to the upper layer when the lower layer vanishes (i.e., $h_2 = 0$). The change of surface and bottom stresses when either layer vanishes is handled by using the Heaviside Step Function $H(h_i)$ ($H(h_i) = 1$ if $h_i > 0$, and $H(h_i) = 0$ if $h_i \leq 0$). Initially, the layer interface is set at 1000 m in the deep basin and at the seafloor, i.e., $h_2 = 0$, wherever the depth is shallower than 1000 m. In each experiment, the model is integrated from an initial state of rest. At 26.5°N, the internal deformation radius is about 50 km for $h_1 =$ 1000 m and $h_2 = 3000$ m. The model has a resolution of 0.25° in a domain from 20°S to 65°N (Figure 1) and uses the ETOPO5 bathymetry data. All lateral boundaries are closed. No-normal flow and no-slip boundary conditions are applied. The model uses a small time step of 10 s.

The AMOC transport at any latitude is defined as the net northward transport between two boundaries in the upper layer, which is virtually identical to the net southward transport in the lower layer. The annual mean overturning transport is zero because there is not water mass fluxes between layers. Two sets of wind stress have been tested in the model, the WHOI OAFlux Wind (which is based on data from several different satellite sensors [*Yu and Jin*, 2010]; http://oaflux.whoi.edu/wind.html) and the ERA-Interim. The evolution of the seasonal variability of the AMOC transport along 26.5°N is very similar when either wind product is used. The peak-to-peak change in AMOC transport at 26.5°N is about 5 and 4 Sv, respectively, when using the OAFlux and ERA-Interim. Both are within the range but smaller than the mean value of 6.7 Sv for 2004–2008 period

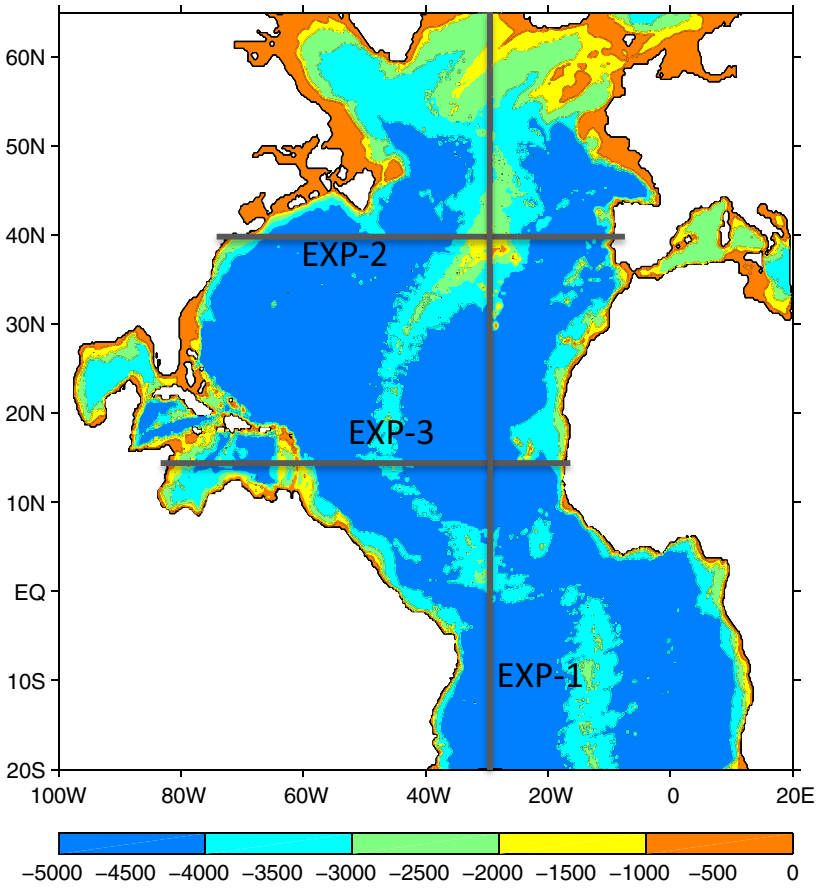

Figure 1. The model domain and bathymetry. In addition to the control run (CTR), three additional experiments (*EXP-1*, 2, and 3) were conducted. In *EXP-1*, a wall is inserted along 30°W. The purpose of this experiment is to examine whether the wind stress curl along the eastern boundary is the predominant forcing for the seasonal variations of the AMOC transport, a hypothesis that was proposed by *Kanzow et al.* [2010]. In *EXP-2* and 3, a wall is inserted along 40°N and 15°N respectively. The purpose is to examine whether the seasonal AMOC variability at 26.5°N is influenced by forcing from the subpolar basin and the tropics.

[*Kanzow et al.*, 2010] and 6 Sv for 2004–2011 [*Zhao and Johns*, 2014]. The results presented in this paper are from simulations that use the OAFlux climatology (1988–2012). The monthly mean stress vector is linearly interpolated to each time step. The model is integrated for 20 years and the output from the twentieth year is used for this study. The model reaches a quasi-equilibrium state within a 20 year spin-up.

3. Seasonal Variability of the AMOC Transport Along 26.5°N

Oceanic data from the RAPID-MOCHA array, together with surface wind stress, allow quantifications of both the mean and variability of the AMOC transport at 26.5°N [*Kanzow et al.*, 2010; *McCarthy et al.*, 2012; *Zhao and Johns*, 2014]. For the seasonal cycle, *Kanzow et al.* [2010] and *Zhao and Johns* [2014] showed that the AMOC transport weakens in spring (March–April) and strengthens in both summer (July) and fall (November). The amplitude of the peak-to-peak change is about 6.7 Sv based on the first 4 years of RAPID-MOCHA data, as indicated by the dashed line in *Kanzow et al.* [2010, Figure 10d]. The error bar, as indicated by the gray envelope in that figure, is inevitably large due to uncertainties in data. The net transport, which is defined as the net northward transport in the upper layer, is comprised of three components, the surface Ekman flow, the western boundary current through the Florida Strait, and the mid-ocean geostrophic flow between the Bahamas and Africa. Kanzow et al. found that the largest contribution to the seasonal variability comes from the mid-ocean geostrophic transport and attributed it to seasonal changes in the eastern boundary pressure (P_E). There is a narrow band of large variations in the wind stress curl off the African coast (their Figure 13a), which, they suggested, is responsible for the seasonal variability of P_E. A baroclinic Rossby-wave model was used to demonstrate the contribution from the eastern-boundary forcing to the AMOC seasonal cycle at 26.5°N.

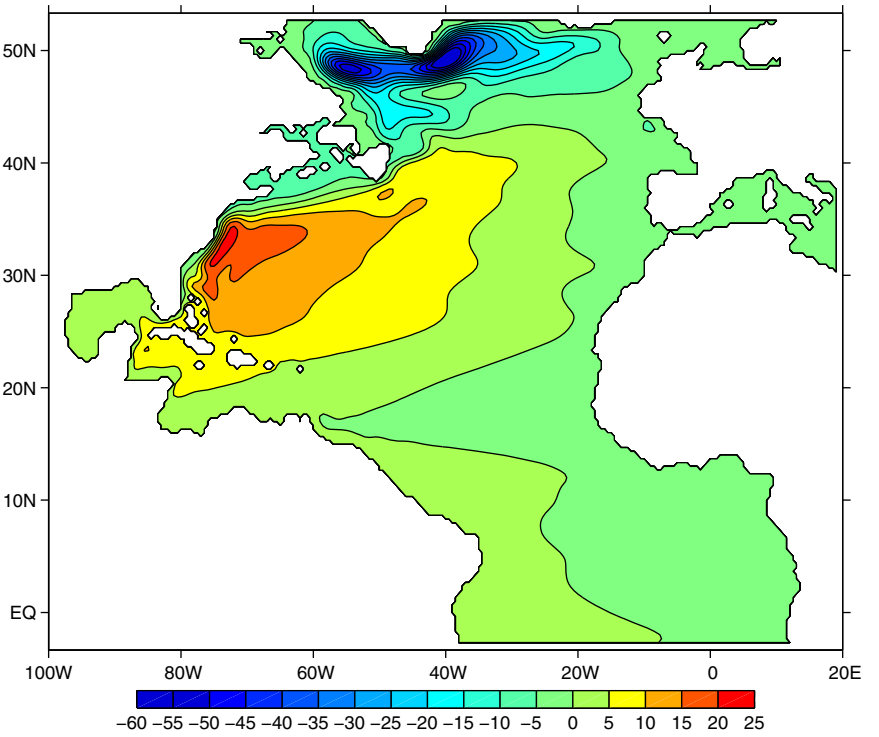

Figure 2. The annual mean sea surface height (SSH, unit: cm) from the twentieth year of the control run (CTR). The OAFlux climatological monthly wind stress (1987–2012) is used in this run. The key feature is the two-gyre system in the North Atlantic Ocean.

In addition to local wind stress, P_E is subject to influences from boundary Kelvin waves and topographic Rossby waves. So it is expected, in terms of wave dynamics, that P_E is also forced by nonlocal wind stress. It is uncertain, however, whether such a contribution from remote forcing to AMOC variability at 26.5°N is comparable to that from the local wind stress. We have designed several experiments to explore this question. But we would like to present the control run first.

3.1. Control Run

The *control run* (*CTR*) is our standard simulation in which no alteration is made in either the bathymetry or the forcing field. It is used to test the model's skill in simulating both the phase and the amplitude of the AMOC seasonal variability at the RAPID-MOCHA Line, and thus to gauge whether this simple model is an appropriate tool for our mechanism study. It is also used for benchmark comparison with results from several sensitivity experiments.

The annual-mean sea surface height (SSH) shows a typical double-gyre feature in the North Atlantic Ocean (Figure 2). The SSH elevation is about 25 cm in the center of the subtropical gyre, which results in a geostrophic transport of about 30 Sv for an upper-layer thickness of 1000 m, consistent with the observed mean Gulf Stream transport of 31.5 Sv at the RAPID-MOCHA array [*Zhao and Johns*, 2014]. The SSH deviation is about 60 cm in the subpolar gyre and the geostrophic transport is about 50 Sv. Both gyres vary seasonally in response to seasonal changes in wind stress. In the lower layer, there is no annual mean circulation after the model is spun-up [*Anderson and Gill*, 1975]. The Anderson-Gill spin-up time scale, defined as the time that a long baroclinic Rossby wave takes to travel from the eastern to the western boundary, is about 4.5 years at 26.5°N for the basin width of about 70° in longitude and a long Rossby wave speed of about 5 cm s^{-1} (the internal deformation radius is about 50 km in the model). So on the seasonal time scale, the circulation in the lower layer does not reach an equilibrium state and continuously adjusts to changes in wind stress forcing.

In the following discussion, we will focus on seasonal changes in the zonally integrated transport. As mentioned above, the AMOC in this purely wind-driven model has no annual-mean transport. The black line in Figure 3 shows the seasonal anomaly of the AMOC transport at 26.5°N, which is defined here as the

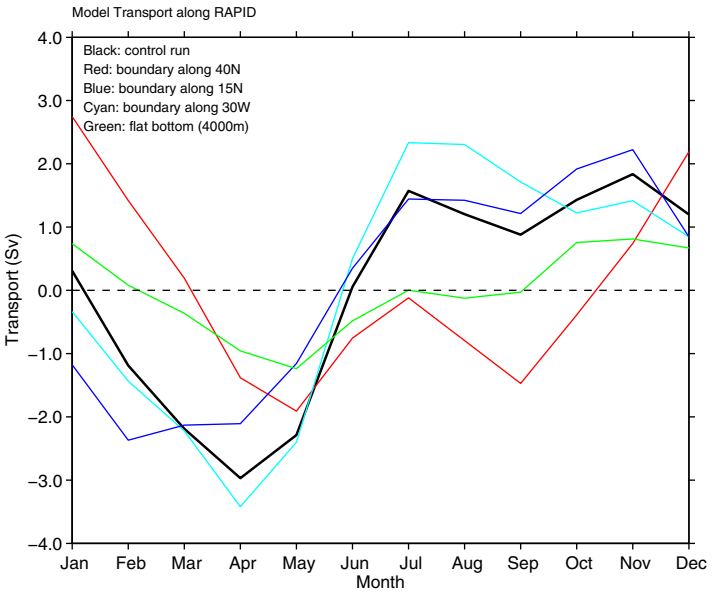

Figure 3. Model transport in the upper layer across the RAPID-MOCHA Line (26.5°N) for *CTR* (black), a run with a wall along 30°W (*EXP-1*, cyan), a run with a wall along 40°N (*EXP-2*, red), and a wall along 15°N (*EXP-3*, blue), and a run with a flat bottom with the depth set to 4000 m everywhere (green). The phase of the seasonal variation in *CTR* (black) agrees with the observation-based estimate [*Kanzow et al*., 2010, Figure 10d].

monthly averaged transport in the upper layer between two boundaries. The phase of this seasonal change agrees very well with the observed one [*Kanzow et al*., 2010, Figure 10d]. In April, the AMOC transport is at its seasonal minimum. It peaks in both July and November just as in the observation-based estimate. The peak-to-peak difference of the AMOC transport between April and November is about 5 Sv in this model run with a climatological forcing. It is considerably lower than the 6.7 Sv that *Kanzow et al*. [2010] estimated for the 2004–2008 period. However, the error bar in the Kanzow et al. estimate (the area enveloped in gray in *Kanzow et al*.'s [2010, Figure 10d]) is large. So the model's 5 Sv transport is still well within the range. *Zhao and Johns* [2014] extended the analysis period of the RAPID-MOCHA observation to 2004–2011 and obtained a peak-to-peak difference of 6 Sv, which is still noticeably higher than the amplitude from our model. It seems typical that models tend to underestimate this amplitude. *Zhao and Johns* [2014] found that the amplitude of the AMOC seasonal change is only about 4 Sv in both the Ocean general circulation model for the Earth Simulator (OFES) and their two-layer model. Given the simplicity of the model, we are satisfied with the agreement between our model and observation-based estimates, and confident that this model can be used for our mechanism study. *Zhao and Johns* [2014] made the same assessment of their two-layer model.

Kanzow et al. [2010] showed that it is the pressure change along the eastern boundary (i.e., African Coast) that dictates the variability in the geostrophic transport [*Kanzow et al*., 2010, Figure 12]. To examine this contribution to the model, we computed Q_g in the upper layer by defining $Q_g = H_0(P_{Africa} - P_{Bahamas})/(\rho_0 f)$, where $H_0 = 1000$ m is the mean thickness of the upper layer and P_{Africa} *and* $P_{Bahamas}$ are the pressure at the eastern boundary and the east coast of the Bahamas in the model. The black line in Figure 4 shows the seasonal anomaly of Q_g. The model's mid-ocean geostrophic transport is indeed a large contributor to the total AMOC seasonal changes. As in the observation [*Kanzow et al*., 2010, Figure 12], both P_{Africa} and $P_{Bahamas}$ make substantial contributions to the total geostrophic transport (red and blue lines in Figure 4). The main feature of the AMOC seasonal cycle is that the transport is weak in spring and strong in fall. This is strongly influenced by the pressure change at the eastern boundary (red line in Figure 4). So the model result is basically consistent with *Kanzow et al*. [2010] assessment that the pressure at the eastern boundary mainly defines the phase of the seasonal cycle in the interior geostrophic transport. The more difficult and still open question is whether P_{Africa} is locally forced.

3.2. Contribution From the Eastern Boundary Pressure to the Seasonal Geostrophic Transport

We conducted a sensitivity experiment (*EXP-1*) in which a large portion of the model domain is blocked from wind stress forcing near the eastern boundary. A thin wall is inserted along 30°W, as indicated as *EXP-1* in Figure 1. This wall effectively separates the model domain into two basins that do not interact with each other. The location of this wall was chosen because a band of large wind stress curl variation is located between 20°W and the African coast [*Kanzow et al*., 2010, Figure 13], and the area to the west of 30°W is well away from this band of wind stress curl. So the meridional overturning circulation (MOC) variability in the western basin in *EXP-1* is not associated with this band of large wind stress curl at the African coast.

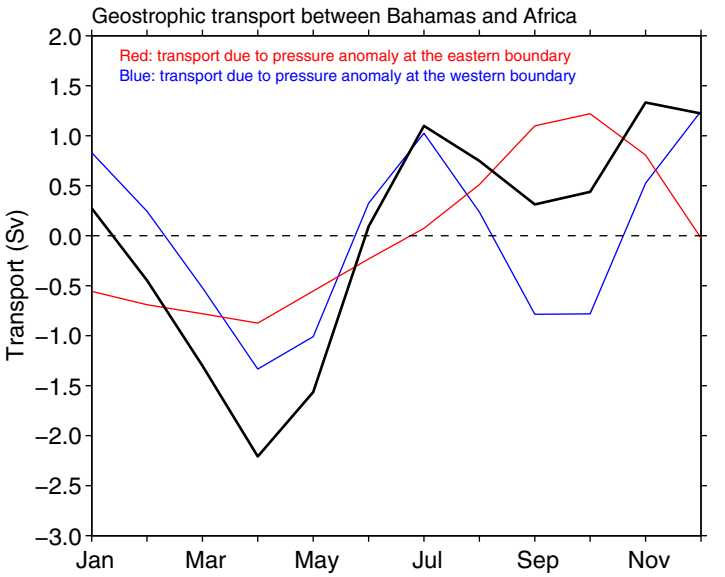

Figure 4. The net northward geostrophic transport in the model between the Bahamas and Africa along 26.5°N (black), and the contribution from pressure along the African (red) and eastern Bahamas (blue) coasts. They are similar to the data-based estimate by *Kanzow et al.* [2010, Figure 12].

With the exception of this artificial wall, the same wind stress and bathymetry that are used in the control run are applied in *EXP-1*. Like that in the control run, the model is integrated for 20 years and the twentieth year result is analyzed here.

Because of the wall at 30°W in *EXP-1*, each basin has its own independent MOC (red and blues lines in Figure 5). The combined transport of the two basin's MOCs at 26.5°N (cyan line in Figure 5 or Figure 3) has a seasonal cycle that is similar to that in *CTR* (black line in Figure 3) except that the summer transport in *EXP-1* is about 0.5–1 Sv higher than that in *CTR*. The presence of the internal wall at 30°W apparently has only a rather small impact on the total AMOC transport at 26.5°N. Even more revealing is the partition of this transport between the two basins. The seasonal MOC variability in the western basin (blue line in Figure 5) not only has a greater amplitude than that in the eastern basin (red), but also makes a greater contribution to the combined MOC transport (cyan line in Figure 5). One could argue that the larger contribution from the western basin simply reflects its proportionality to its larger width at 26.5°N. The important point to emphasize here, however, is that this large MOC variability in the western basin is not related to the band of large wind stress curl at the African coast, indicating that the eastern boundary forcing may not be

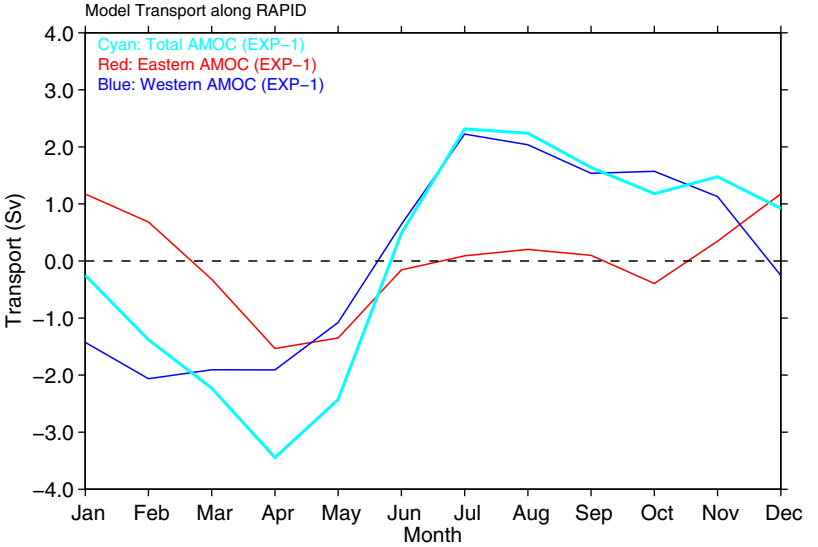

Figure 5. The AMOC seasonal transports at 26.5°N from *EXP-1* with a wall at 30°W (red and blue lines for the eastern and western basin, respectively, and the cyan line is for the combined transport of two basins). The combined transport is close to that in the control run (black line in Figure 3), indicating that a wall at 30°W does not significantly affect the seasonal cycle of the AMOC transport at 26.5°N. The transport at the western basin is robust and makes a greater contribution to the combined transport than that from the eastern basin. This indicates that the wind stress curl at the eastern boundary is not the predominant forcing of the seasonal variability of the AMOC at 26.5°N.

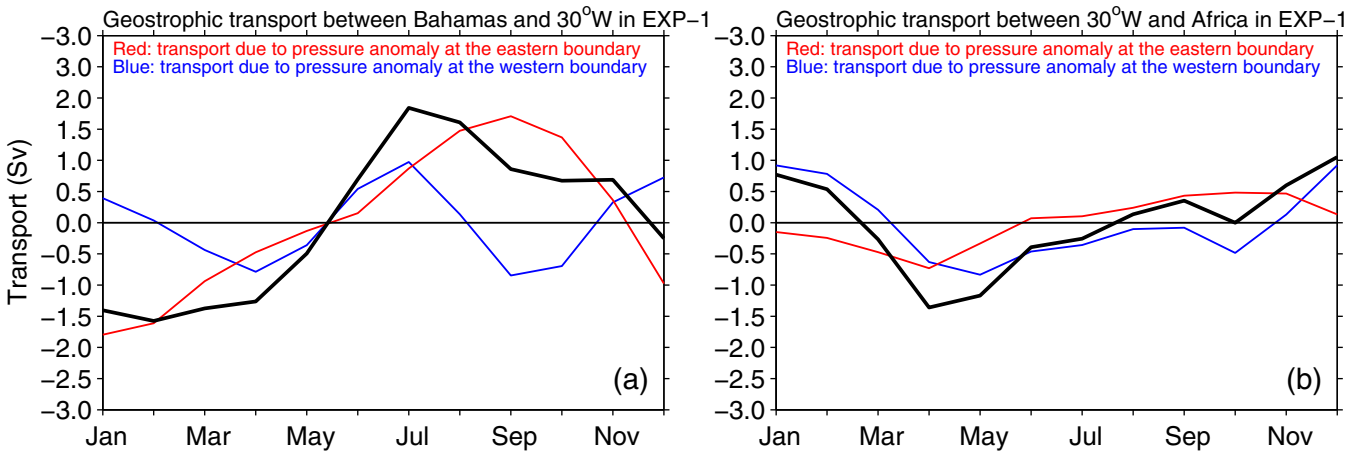

Figure 6. Geostrophic transport from *EXP-1* (with an internal wall along 30°W). (a) The geostrophic transport between the Bahamas and the inserted 30°W wall (black). The red line and blue lines are contributions from the pressure anomaly from the western and eastern boundaries. (b) The geostrophic transport in the eastern basin (black) and contributions from pressure at the western (blue) and eastern (red) boundaries. Note that the contribution from the pressure anomaly at the African coast is much smaller in this experiment than that in the control run (red line in Figure 4). The pressure anomaly at the eastern boundary in the western basin (red line in the left plot), however, is similar to the pressure anomaly at the African coast in the control run (red line, Figure 4). This again indicates that the pressure anomaly at the eastern boundary is not mainly forced by the local wind stress.

the only major forcing mechanism for the observed seasonal variability of the AMOC transport at the RAPID-MOCHA array.

We calculate the geostrophic transport in each basin by using $Q_g = H_0(P_{east} - P_{west})/(\rho_0 f)$, where P_{east} and P_{west} are pressure at the eastern and western boundaries in each basin and $H_0 = 1000$ m is the mean upper-layer thickness. The geostrophic transports from *EXP-1* are shown in Figures 6a and 6b. The red and blue lines depict the contributions to the geostrophic transport from the pressure at the eastern and western boundary in each basin respectively. It is worth noting that the pressure variability at the African coast in the eastern basin (red, Figure 6b) becomes much smaller than that in the control run (red line, Figure 4). In contrast, the pressure at the western basin's eastern boundary (i.e., the western side of the inserted wall at 30°W) makes a major contribution to the overall geostrophic transport (red line, Figure 6a). The large variability of the wind stress curl off the African coast cannot affect processes in the western basin due to the wall at 30°W in the model. The similarity between red lines in Figure 6a (pressure at the western basin's eastern boundary in *EXP-1*) and Figure 4 (pressure at the African coast in the control run) suggests that the pressure change at the African coast in the *CTR* is not forced locally. It must be due to either the integrated forcing across the basin at 26.5°N or the remote influences from different latitudes. Note that the small seasonal AMOC variability in the eastern basin in *EXP-1* is not due to a lack of large wind stress curl at the eastern boundary. Both the pattern and the magnitude of the wind stress curl at 26.5°N are very similar to what was shown in Figure 13 of *Kanzow et al.* [2010].

3.3. Contributions From the Subpolar Basin and the Tropics

The ocean circulation adjusts to an external forcing through propagation of planetary, topographic, and gravity waves. These waves spread oceanic responses, typically in the form of pressure anomalies, around the basin, and induce anomalous velocities along wave pathways. This is the essence of remote forcing or teleconnection mechanisms that were discussed in many previous studies [e.g., *Yu et al.*, 1991; *Johnson and Marshall*, 2002; *Yang*, 1999]. The RAPID-MOCHA array at 26.5°N is located in the subtropical basin. We are interested in whether the seasonal AMOC variability at 26.5°N is influenced by wind stress forcing in the subpolar basin and in the tropics. We decided to conduct two additional sensitivity experiments to explore this remote forcing mechanism. In *EXP-2*, a wall is placed along 40°N (Figure 1) to block remotely forced signals that originated in the subpolar basin from reaching 26.5°N. In *EXP-3*, a wall along 15°N (Figure 1) restricts forcing from the tropics. Other than the insertion of internal walls, everything else in *EXP-2* and *EXP-3*, is kept the same as in *CTR*. Any difference in these two experiments from the control run, therefore, is due to the insertion of internal walls.

The red and blue lines in Figure 3 show the AMOC transports at 26.5°N from *EXP-2* and *EXP-3*, respectively. For comparison, the black line in the same figure shows the AMOC transport from *CTR*. The internal wall at

40°N in *EXP-2* clearly affects both the amplitude and the phase of the seasonal variability of the AMOC transport at the RAPID-MOCHA Line. In comparison with *CTR* (black line), the AMOC transport in *EXP-2* (red line) becomes weaker from May to November, and stronger between December and May. Likewise, placing a wall at 15°N in *EXP-3* also affects the AMOC transport at 26.5°N although to a lesser extent (comparing blue and black lines in Figure 3). The AMOC seasonal cycle at 26.5°N would change differently if the wall were shifted to different latitudes. But it is already obvious from *EXP-2* and *EXP-3* that the seasonal cycle of the AMOC transport at the RAPID-MOCHA Line is not forced only by the local forcing at 26.5°N since the forcing at this latitude is the same in all experiments.

We would like to point out that inserting walls is an intrusive method that changes the basin-wide circulations. We tried two other methods of separating forcing from a particular region. One is to simply use the annual-mean wind stress in one particular region, such as in the area to the north of 40°N. This method has a large seasonal anomaly of wind stress curl at 40°N and results in strong localized recirculation at this latitude. The second alternative method is to adjust wind stress in the region to the north of 40°N to avoid discontinuity of the curl. The meridional component of the wind stress is set to their annual mean field, i.e., $\tau^y(x,y,t) = \tau_0^y(x,y)$. The zonal component consists of the annual mean wind stress and the seasonal anomaly at 40°N, i.e., $\tau^x(x,y,t) = \tau_0^x(x,y) + \tau_{anomaly}^x(x,y_{40N},t)$. The subscript 0 refers to the annual mean fields. In this arrangement, the wind stress curl anomaly is zero in the area to the north of 40°N. The AMOC transports at 26.5°N from these two experiments are quite similar to that shown in *EXP-2* with an artificial wall inserted at 40°N.

How does wind stress in the subpolar basin or in the tropics affect the AMOC transport in the subtropical basin? Our two-layer model has no diapycnal flux, and so the water volume in each layer is conserved. But the spatial distribution of the water mass in each layer varies seasonally. In the upper layer, for instance, a convergence of the volume transport in the subpolar basin requires a transport divergence elsewhere. This wind-driven movement results in a seasonal variability in the upper limb of the AMOC. How about the lower limb, i.e., the transport of the NADW layer? In a two-layer system, transport variations in the upper and lower layers are tightly coupled. The total water volume from the sea surface to the seafloor in a given area is nearly constant since seasonal SSH variability, which is in the range of several centimeters, has a negligible effect. A convergence in the upper-layer transport deepens the pycnocline (or the layer interface in a two-layer model) and squeezes the volume in the lower layer. Therefore, there must be a divergent transport in the lower layer to balance a convergence in the upper layer. Through this coupling, wind stress forces variations in the lower limb of the AMOC.

Seasonal variations in the model's AMOC transport are driven by the Ekman pumping/suction as illustrated in Figure 7. Consider a season when the wind stress curl is anomalously positive in the subpolar basin. The anomalous Ekman suction uplifts the layer interface, and results in a water-volume increase in the lower layer and decrease in the upper layer. This leads to an anomalous northward flow in the lower layer from the subtropical basin to the subpolar basin, and a transport in the opposite direction in the upper layer. This anomalous sheared transport, i.e., southward in the surface layer and northward in the bottom layer, is opposite to the mean buoyancy-driven AMOC (which is absent in this wind-driven model). So the strengthening Ekman suction in the subpolar basin would result in a negative anomaly in the AMOC transport, and vice versa for an opposite anomaly in wind stress curl. The same mechanism also works for remote forcing from the tropics and explains why the AMOC transport at 26.5°N changes when a wall is inserted at 15°N in *EXP-3*. Through this mechanism, the AMOC transport at 26.5°N is responsive to changes in wind stress forcing in other latitudes even if the wind stress remains unchanged locally. We would like to point out that Figure 7 depicts a mechanism for the zonally integrated transport. Transport anomaly that is induced by the Ekman pumping in the interior and at the eastern boundary would propagate westward by Rossby waves and result in changes in boundary current transport.

The wind stress curl in the subpolar basin is basically the opposite of that in the subtropics as shown in Figure 8. An anomalous suction in the subpolar basin is accompanied by a pumping in the subtropics. As shown in Figure 7, a strengthening Ekman pumping in the subtropics also weakens the AMOC transport, and vice versa for the subtropical suction. Therefore, the seasonal variability of the AMOC transport in the North Atlantic Ocean, including that at 26.5°N, is forced by the Ekman pumping/suction in the whole basin, not just in one particular area. This mechanism (Figure 7) also explains why a meridional wall, like the one inserted along 30°W in *EXP-1*, does not block this meridional redistribution of layer volumes and therefore has little impact on the net AMOC transport.

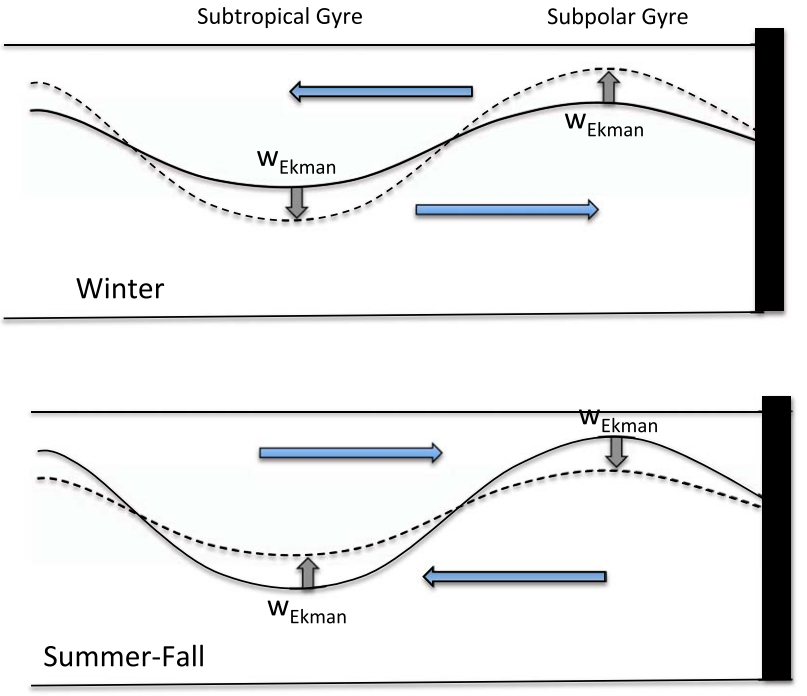

Figure 7. The schematics of interactions between subtropical and subpolar gyres. (top) There is southward transport in the upper layer when either the Ekman pumping in the subtropics or Ekman suction in the subpolar basin intensifies. This would lead to a weakening of the mean AMOC. (bottom) Likewise, the AMOC would increase when either the Ekman pumping in the subtropics or suction in the subpolar basin weakens.

Now let us examine whether the mechanism schematized in Figure 7 is consistent with the seasonal variability of the wind stress curl. Figure 8 shows the seasonal anomaly of the zonally integrated wind stress curl from 20°S to 65°N. From April to November, the wind stress curl is anomalously negative in the subpolar basin north of 55°N and positive in the subtropics between 20°N and 40°N (Figure 8). As illustrated in Figure 7, this contrast of wind stress curl forces a northward transport in the upper layer from the subtropical to subpolar basin and strengthens the AMOC transport. The seasonal change reverses in the period between November and March when the wind stress curl anomaly changes the sign in both the subpolar and subtropical basins.

The upper-layer volume in the model between 40°N and 65°N (red line in Figure 9a) indeed increases from May to November and decreases from November to March, a 1-month lag to the wind stress curl. The spatial patterns of anomalous thickness of the upper layer in April and November are shown in Figure 9b. The thickness change in either month is not spatially uniform. Larger changes are located mainly in the western side of the subpolar basin in the Irminger Sea, Labrador Seas, and along the western boundary current. But it is quite clear that the upper-layer volume north of 40°N is low in April and high in November. The black line in Figure 9 indicates the upper-layer volume in the subtropical basin between 15°N and 40°N. Its phase evolution is the opposite of that in the subpolar basin (red line), supporting the mechanism illustrated in Figure 7.

The two plots in Figure 9b show that planetary Rossby waves, characterized as southwest-to-northeast tilted bands of h_1 anomalies, move westward in the region to the south of about 50°N. But they seem to be absent in the subpolar basin. For linear Rossby waves, there is a turning latitude θ_c for a given frequency ω. Planetary Rossby waves with a frequency at or higher than ω cannot exist in the areas poleward of the turning latitude θ_c. This theoretical result, which is discussed in many textbooks, has been tested using satellite altimetry data and outputs of high-resolution ocean models [*Lin et al.*, 2008, 2014]. In our simulations with monthly climatological wind stress, the lowest frequency in the model is $\omega = 2\pi/(12 \text{ months})$. So planetary Rossby waves exist only in latitudes that are lower than the turning latitude associated with the annual period. The critical latitude is defined as:

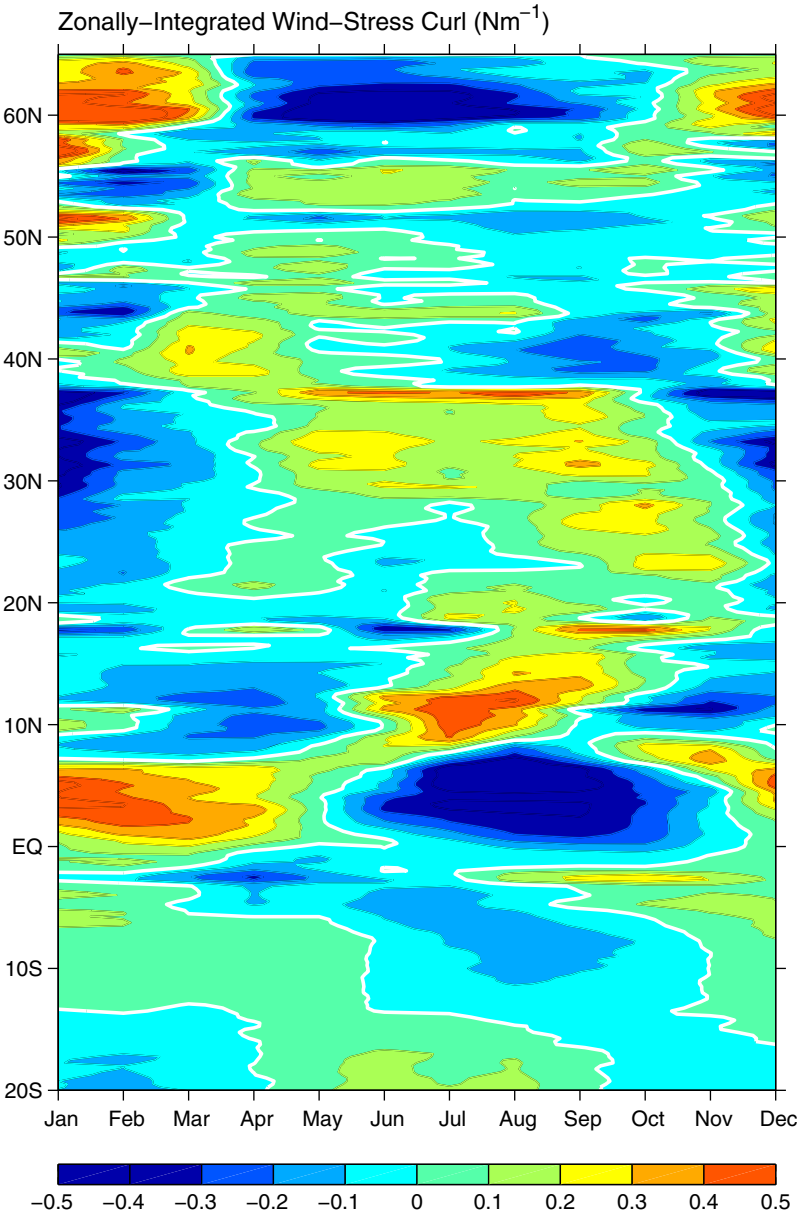

Figure 8. Hovmoller diagram of the zonally integrated wind stress curl across the whole basin.

$$\theta_c = \cot^{-1}\left(\frac{2R\omega}{c_1}\right) \tag{2}$$

where R is earth's radius and $c_1 = \left[\frac{g\Delta\rho h_1 h_2}{\rho(h_1+h_2)}\right]^{1/2}$ is the first baroclinic Kelvin wave speed. For $h_1 = 1000$ m, $h_2 = 3000$ m, and $\Delta\rho = 1.5$ kg m^{-3}, the Kelvin wave speed is about 3.3 m s^{-1}. The turning latitude for $\omega = 2\pi$/(12 months), according to equation (2), is about 52° in latitude. So the latitudinal distribution of planetary Rossby waves in Figure 9 is consistent with the dispersion relation of linear waves. But we should note that h_1 and h_2 are not constant due to varying topography, and the position of θ_c varies.

3.4. Latitudinal Coherence

Previous studies suggest that the AMOC transport should vary coherently across latitudes. Such coherences, however, may not be continuous across all latitudes [*Bingham et al.*, 2007] and could depend on pathways of NADW export [*Zhang*, 2010]. The latitudinal coherence of the AMOC transport in the control run is

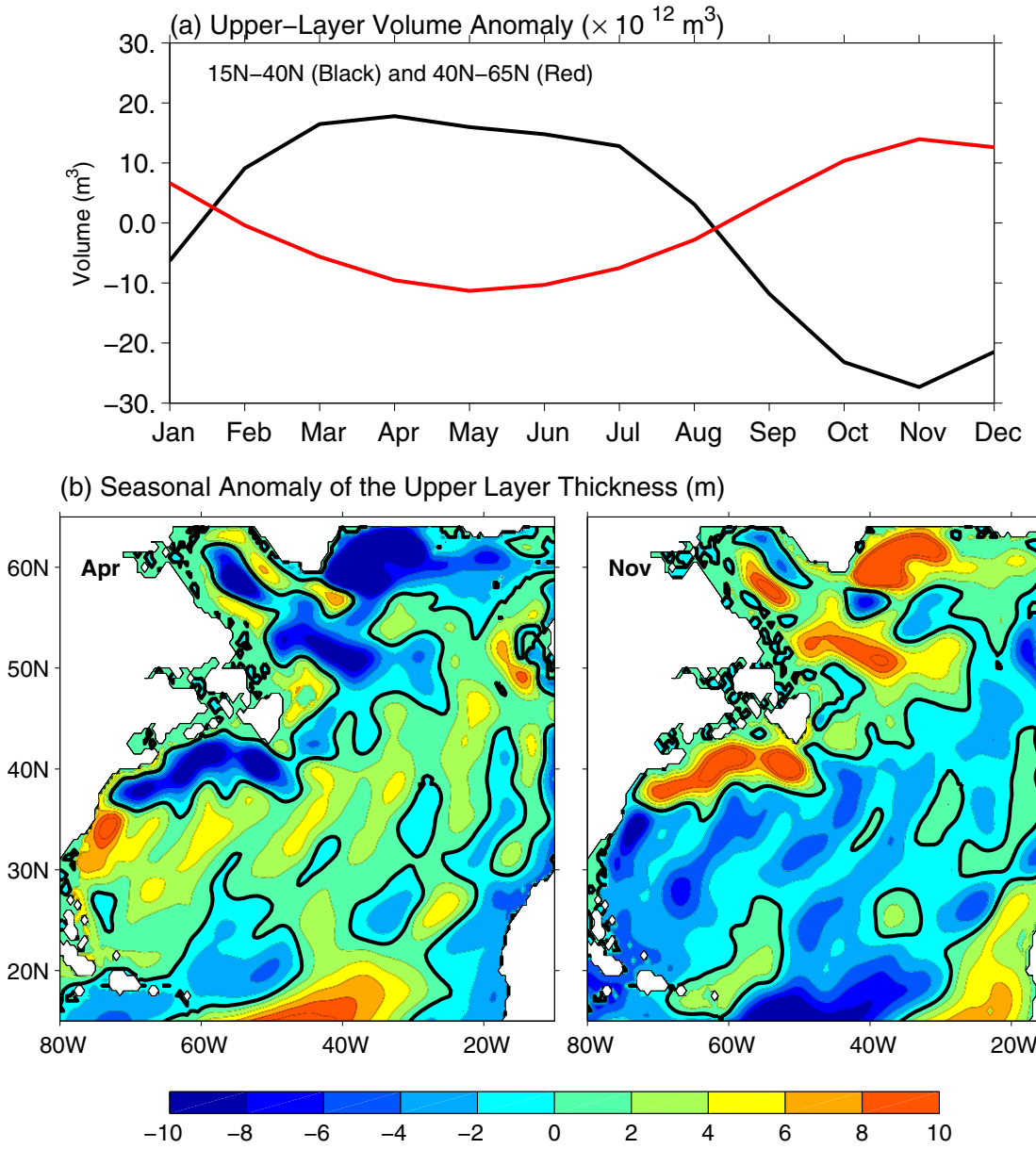

Figure 9. (a) The seasonal variation of the upper-layer water mass volume between 15°N and 40°N (black line) and between 40°N and 65°N (red line); the seasonal anomaly of the upper-layer thickness h_1 (b) in April and (c) in November.

illustrated in the Hovmoller (latitude-time) diagram of the AMOC transport (Figure 10a). The pattern is quite similar to that of a high-resolution OGCM simulation discussed by *Mielke et al.* [2013] and *Xu et al.* [2014]. As pointed out by *Mielke et al.* and also shown in Figure 10a, the AMOC transport is meridionally covariable between the subtropical and subpolar basins. Figure 10 shows that the seasonal variability of the AMOC transport in the subpolar basin leads that in the subtropics. The phase of the seasonal anomaly moves southward between 25°N and 65°N. *Mielke et al.* [2013] also showed a phase shift of the seasonal cycle at 41°N, computed by using altimetry and ARGO float data [*Willis*, 2010], and at the RAPID-MOCHA array.

An internal wall at 40°N in *EXP-2* clearly affects the polar-subtropical interactions and the latitudinal coherence of the AMOC seasonal cycle (Figure 10b). The AMOC transport over the whole subtropical basin becomes much weakened when compared with that in the control run (Figure 10a). It is interesting to note that both the amplitude and the phase of the seasonal variability changes much less significantly in the

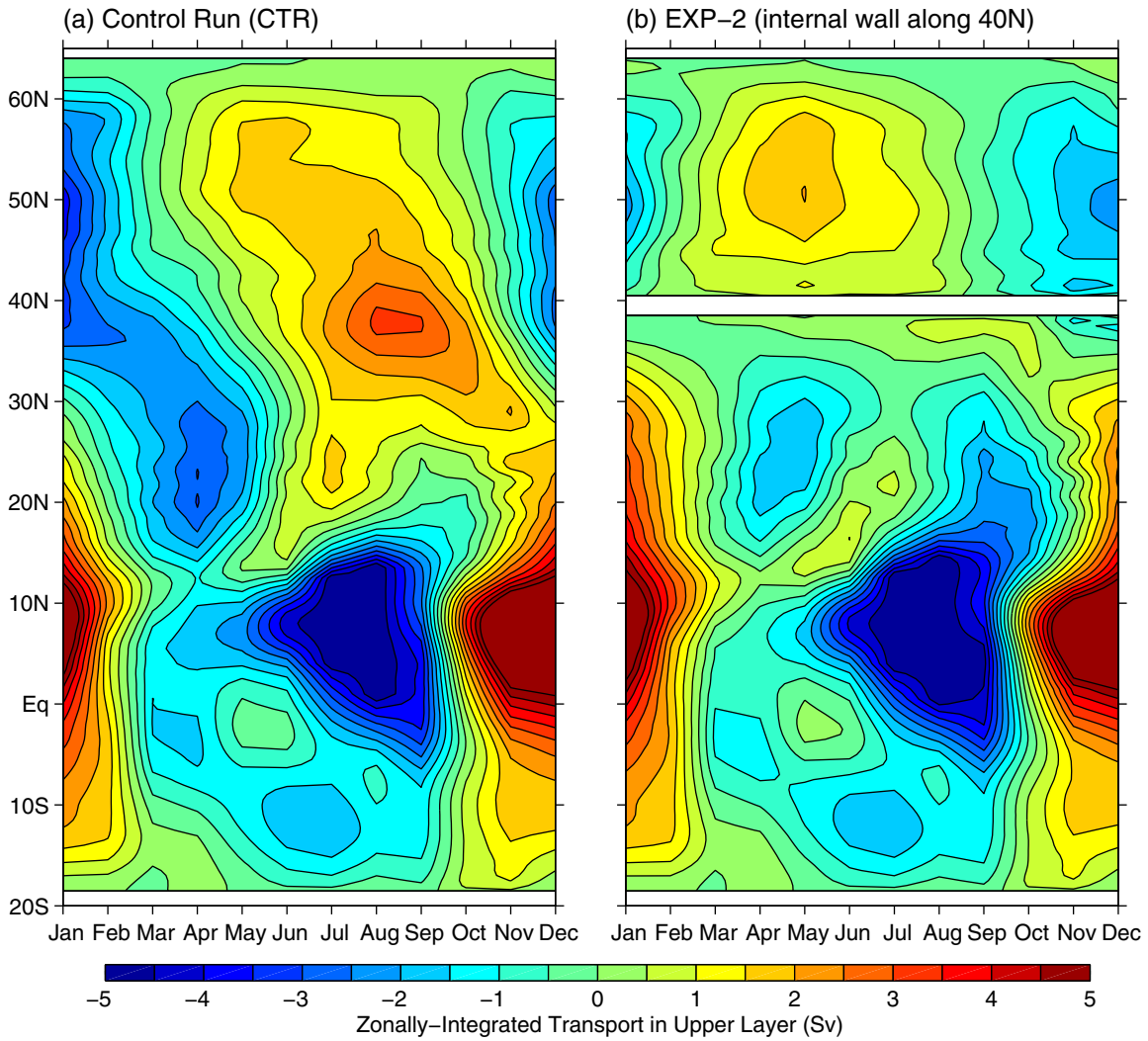

Figure 10. The seasonal variations of the zonally integrated northward transport in the upper layer for (a) the control run and (b) *EXP-2*. In *EXP-2* (right), the internal wall blocks interactions between the subtropical and subpolar basins and strongly affects the transport along 26.5°N.

subpolar basin than in the subtropics by the insertion of the wall. The seasonal cycle in the region north of the wall at 40°N only shifts by 1 month and the amplitude weakens by about 10–15% (Figure 10b). The change is much greater in the subtropics. This contrast implies that the wind stress forcing in the subpolar basin exerts a greater influence on the AMOC seasonal cycle in the subtropics than the influence of subtropical wind stress on the AMOC variability in the subpolar basin.

3.5. Barotropic and Some Topographic Effects on the Seasonal Variability in AMOC Transport

The mechanism illustrated in Figure 7 includes Sverdrup transport that is forced by the Ekman pumping and suction. The Sverdrup balance is an instantaneous and barotropic response to wind stress curl. So topography is expected to be important in the model's adjustment to the seasonally changing wind stress. But the AMOC is a vertically sheared overturning cell and thus is inherently baroclinic. Does the barotropic mode play a role in the seasonal AMOC variability? To explore this, we ran an additional experiment by using a constant depth everywhere at 4000 m. The basin's coastline and wind stress remain the same as in *CTR*. The green line in Figure 3 shows the seasonal cycle of the AMOC transport along 26.5°N. The amplitude of the seasonal variations is much smaller than that in *CTR*. Topography affects oceanic responses in multiple ways to be discussed in the following.

We decompose the annual variability of the AMOC transport at 26.5°N in *CTR* to both the barotropic mode, which is defined as $\overrightarrow{u}^{BT}=\left(h_1\overrightarrow{u}_1+h_2\overrightarrow{u}_2\right)/(h_1+h_2)$, and baroclinic mode, which is expressed as

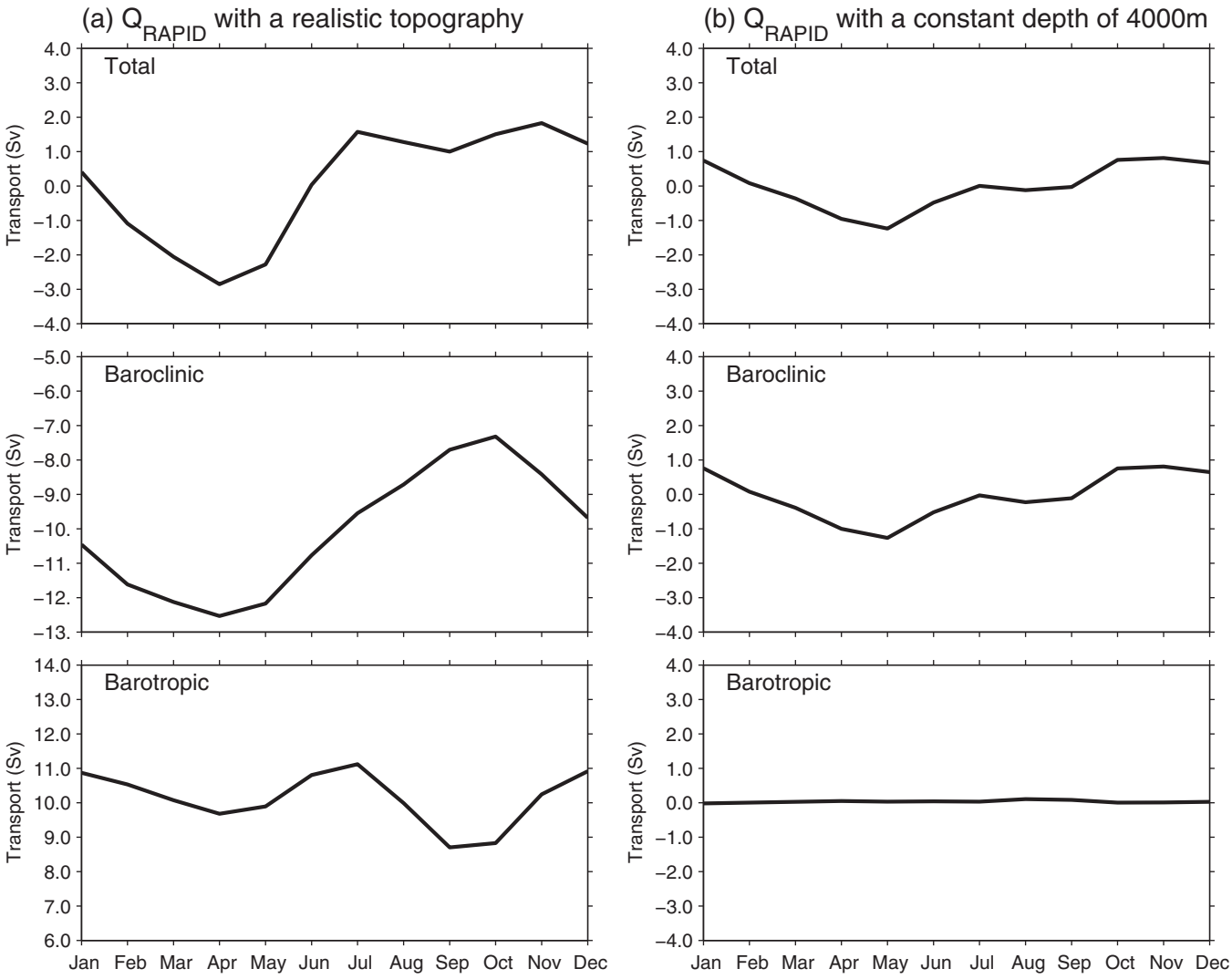

Figure 11. (top) The seasonal evolution of the AMOC transport at 26.5°N, its (middle) baroclinic and (bottom) barotropic components (left) from the control run and (right) from a flat-bottom simulation (a constant depth at 4000 m). Note that barotropic transport makes no contribution in a flat bottom model (bottom right). But it makes a significant contribution when topography is included in the model (bottom left).

$\overrightarrow{u}_n^{BC} = \overrightarrow{u}_n - \overrightarrow{u}^{BT}$ (where n denotes the nth layer). We defined their contributions to the AMOC variability by their contribution to the zonally integrated northward transport in the upper layer. As shown in Figure 11 (left), the seasonal variations of the barotropic and baroclinic components are in phase from January to July, i.e., both transports decrease from January to April and then increase from April to July. The baroclinic transport continues to increase until it peaks in October. The barotropic transport, however, decreases from July to September before it increases again from September to December.

It is interesting to note that the evolution of the baroclinic transport is very similar to the mid-ocean transport that was obtained by *Kanzow et al.* [2010] (blue line in their Figure 14) who used a linear model for long baroclinic Rossby waves. The peak-to-peak change in the baroclinic transport is about 5.5 Sv (middle, Figure 11, left). This is about the same as that from Kanzow et al. wave model. But the transport in our model includes both the interior and the western boundary current (WBC) transports, while Kanzow et al. model simulates only the mid-ocean geostrophic transport. So they are not exactly comparable even though the two transports are quite similar.

We have analyzed the barotropic and baroclinic transports in our sensitivity experiments, i.e., *EXP-1, 2,* and *3*. The amplitude of the seasonal variability in the baroclinic transport is reduced to 3 Sv (not shown) in *EXP-2* when an internal wall is inserted along 40°N, indicating that the baroclinic transport itself is

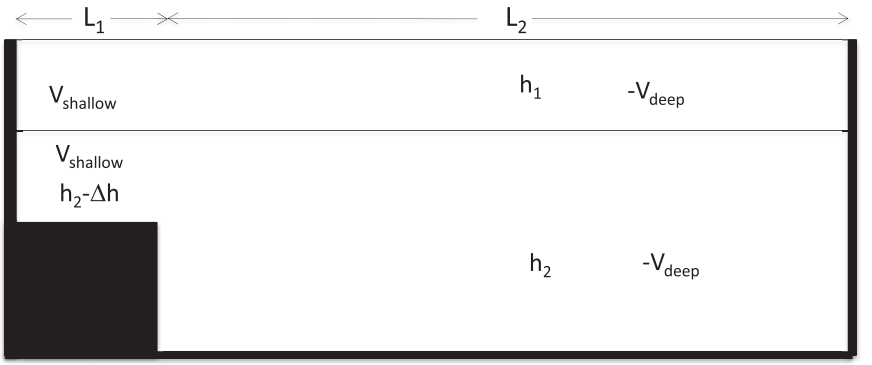

Figure 12. A schematic to illustrate how topography affects a barotropic gyre resulting in its contribution to variations in the AMOC transport.

influenced by remote forcing from the subpolar basin. Our analyses also show that the wind stress forcing to the east of the mid-ocean ridge contributes to the season variability of the AMOC transport. Kanzow et al. excluded the forcing to the east of 50°W in their calculation by assuming that baroclinic waves would be blocked by the ridge and therefore do not affect the pressure at the western boundary.

How does the barotropic mode contribute to the variability of the AMOC – an inherently baroclinic circulation? Here we use a schematic to illustrate how barotropic flows affect the AMOC transport variability. We examine a barotropic circulation in a basin that has a flat bottom in the interior and a step-like shelf off the western boundary (Figure 12). It is assumed that the WBC occupies the whole shelf. The total interior transport between $x = L_1$ and $x = L_1 + L_2$ is $Q_i = (h_1 + h_2)\, L_2 V_{deep}$, assuming that the interior velocity is constant in x. The transport of the WBC is $Q_w = (h_1 + h_2 - \Delta h) L_1 V_{shallow}$. The mass conservation requires that $Q_i = Q_w$, and so a relationship between two velocities can be obtained:

$$L_2 V_{deep} = \left(1 - \frac{\Delta h}{h_1 + h_2}\right) L_1 V_{shallow} \tag{3}$$

The net northward transport in the upper layer or the southward transport in the lower layer is:

$$\Delta Q = h_1 (L_1 V_{shallow} - L_2 V_{deep}) = \frac{h_1 \Delta h}{h_1 + h_2} (L_1 V_{shallow}) \neq 0 \tag{4}$$

So the barotropic flow depicted in Figure 12 has a northward nontrivial transport of ΔQ in the upper layer and a southward one in the lower layer. Such a transport vanishes in a flat bottom model since $\Delta h = 0$. It is worth noting that there are convergence and divergence of volume transports in either layer when $\Delta Q \neq 0$, and such convergence/divergence would deform the layer interface. Such changes in pycnocline depth initiate baroclinic processes that further affect the AMOC transport. The role of topography in inducing overturning variability through wind-driven gyres has been discussed in several previous studies in various ocean regions [e.g., *Lee and Marotzke*, 1998; *Hakkinen*, 2001; *Cabanes et al*., 2008].

4. Discussion and Summary

In this paper, we describe a two-layer and adiabatic model that is driven by a climatological wind stress to investigate whether remote wind stress forcing contributes to the seasonal variability of the AMOC transport at 26.5°N. Our model result agrees with previous studies that the pressure at the eastern boundary is a main contributor for changes in the mid-ocean geostrophic transport [*Kanzow et al*., 2010; *Zhao and Johns*, 2014], which itself is the largest contributor to the AMOC annual cycle at 26.5°N. But our results, in contrast to Kanzow et al. study, indicate that the pressure at the eastern boundary is not forced mainly by the local wind stress curl at the African coast. It is as a result of the basin-wide adjustments to both local and remote wind stress forcing. In *EXP-1*, a wall was inserted to block the wind stress curl near the eastern boundary from forcing the basin to the west of 30°W. The AMOC seasonal variability in the western basin remains robust and resembles that of the control run even though the western basin is not forced by the wind stress curl at the eastern boundary. Furthermore, the pressure at the western side of the wall, i.e., the eastern

boundary of the western basin, varies significantly with the season and contributes to the seasonal cycle of the geostrophic transport in the western basin. We conclude that this boundary pressure variability, like the one at the African coast in the control run, is primarily due to basin-wide adjustments. The seasonal variability of the AMOC transports in the subtropical and subpolar basins are intimately linked through meridional redistribution of water masses in each layer. Two additional experiments were conducted to elucidate this connection. In *EXP-2*, an internal wall was inserted at 40°N to block forcing from the area north of this latitude. The local forcing and bathymetry at 26.5°N are the same as that in the control run. The AMOC transport was substantially changed, indicating the role a high-latitude forcing has on the subtropics. A similar experiment, *EXP-3*, was conducted by putting a wall at 15°N to block forcing from the tropics. The AMOC transport at 26.5°N was affected considerably although not as profoundly as that in *EXP-2*. The leading mechanism in our model for the seasonal variability of the AMOC transport at 26.5°N is illustrated in Figure 7. A weakening Ekman suction in the subpolar basin or pumping in the subtropical basin leads to an anomalous northward transport in the upper layer and a southward one in the lower layer. This strengthens the mean AMOC transport that is driven by the deep-water formation/removal processes (not included in the model).

Barotropic processes play an important role in the seasonal variability of the AMOC transport through topography-gyre interactions. Barotropic transports in a stratified ocean with a varying depth can induce a convergence of divergence of water mass volume in a density layer within an area. This leads to a temporal change in the AMOC transport as schematized in Figure 12. Baroclinic responses follow immediately once such a divergence/convergence occurs. The adjustment would likely involve complex interactions between barotropic and baroclinic modes as discussed by *Andres et al*. [2012]. It requires further study to understand such interactions. The purpose here is to point out the role of barotropic processes in the seasonal AMOC transport at 26.5°N. Previous studies have emphasized mainly baroclinic Rossby waves that are forced locally by the wind stress curl.

Acknowledgment
This study has been supported by the National Science Foundation (OCE 0927017). The author is grateful to three reviewers for their constructive and very useful comments and suggestions. To access the model code and the forcing data, please e-mail the author, jyang@whoi.edu

References

Anderson, D. T. L., and A. E. Gill (1975), Spin-up of a stratified ocean, with applications to upwelling, *Deep Sea Res. Oceanogr. Abstr.*, *22*, 583–596.

Andres, M., J. Yang, and Y. O. Kwon (2012), Adjustment of a wind-driven two-layer system with mid-basin topography, *J. Mar. Res.*, *70*(6), 851–882.

Biastoch, A., C. W. Boning, and J. Getzlaff (2008), Causes of interannual–decadal variability in the meridional overturning circulation of the midlatitude North Atlantic Ocean, *J. Clim.*, *21*, 6599–6615.

Bingham, R. J., C. W. Hughes, V. Roussenov, and R. G. Williams (2007), Meridional coherence of the North Atlantic meridional overturning circulation, *Geophys. Res. Lett.*, *34*, L23606, doi:10.1029/2007GL031731.

Cabanes, C., T. Lee, and L.-L. Fu (2008), Mechanisms of interannual variations of the Meridional Overturning circulation of the North Atlantic Ocean, *J. Phys. Oceanogr.*, *38*, 467–480.

Chidichimo, M. P., T. Kanzow, S. A. Cunningham, and J. Marotzke (2010), The contribution of eastern boundary density variations to the Atlantic meridional overturning circulation at 26.5N, *Ocean Sci.*, *6*, 475–490.

Cunningham, S. A., et al. (2007), Temporal variability of the Atlantic meridional overturning circulation at 26.5N, *Science*, *317*, 935–938.

Hakkinen, S. (2001), Variability in sea surface height: A qualitative measure for the meridional overturning in the North Atlantic, *J. Geophys. Res.*, *106*, 13,837–13,848.

Johns, W. E., L. M. Beal, M. O. Baringer, J. R. Molina, S. A. Cunningham, T. Kanzow, and D. Rayner (2008), Variability of shallow and deep western boundary currents off the Bahamas during 2004–05: Results from the 26°N RAPID–MOC array, *J. Phys. Oceanogr.*, *38*, 605–623.

Johns, W. E., et al. (2011), Continuous, array-based estimates of Atlantic Ocean heat transport at 26.5°N, *J. Clim.*, *24*, 2429–2449.

Johnson, H. L., and D. P. Marshall (2002), A theory for the surface Atlantic response to thermohaline variability, *J. Phys. Oceanogr.*, *32*, 1121–1132.

Kanzow, T., et al. (2010), Seasonal variability of the Atlantic Meridional Overturning Circulation at 26.5°N, *J. Clim.*, *23*, 5678–5698.

Kawase, M. (1987), Establishment of deep ocean circulation driven by deep-water production, *J. Phys. Oceanogr.*, *17*, 2294–2317.

Lee, T., and J. Marotzke (1998), Seasonal cycles of meridional overturning and heat transport of the Indian Ocean, *J. Phys. Oceanogr.*, *28*, 923–943.

Lin, X., J. Yang, D. Wu, and P. Zhai (2008), Explaining the global distribution of peak-spectrum variability of sea surface height, *Geophys. Res. Lett.*, *35*, L14602, doi:10.1029/2008GL034312.

Lin, X., Y. Yi, P. Zhai, and J. Yang (2014), A mechanism for the latitudinal dependence of peak-spectrum sea surface height variability, *J. Geophys. Res. Oceans*, *119*, 1431–1444, doi:10.1002/2013JC009642.

McCarthy, G., E. Frajka-Williams, W. E. Johns, M. O. Baringer, C. S. Meinen, H. L. Bryden, D. Rayner, A. Duchez, C. Roberts, and S. A. Cunningham (2012), Observed interannual variability of the Atlantic meridional overturning circulation at 26.5°N, *Geophys. Res. Lett.*, *39*, L19609, doi:10.1029/2012GL052933.

Meinen, C. S., M. O. Baringer, and R. F. Garcia (2010), Florida Current transport variability: An analysis of annual and longer period signals, *Deep Sea Res., Part I*, *57*, 835–846, doi:10.1016/j.dsr.2010.04.001.

Meinen, C. S., W. E. Johns, S. L. Garzoli, E. van Sebille, D. Rayner, T. Kanzow, and M. O. Baringer (2013), Variability of the Deep Western Boundary Current at 26.5°N during 2004–2209, *Deep Sea Res., Part II*, *85*, 154–168.

Mielke, C., E. Frajka-Williams, and J. Baehr (2013), Observed and simulated variability of the AMOC at 26°N and 41°N, *Geophys. Res. Lett.*, *40*, 1159–1164, doi:10.1002/grl.50233.

Polo, I., J. Robson, R. Sutton, and M. Balmaseda (2014), The importance of wind and buoyancy forcing for the boundary density variations and the geostrophic component of the AMOC at 26°N, *J. Phys. Oceanogr.*, *44*, 2387–2408, doi:10.1175/JPO-D-13-0264.1.

Veronis, G., and H. Stommel (1956), The action of variable wind stresses on a stratified ocean, *J. Mar. Res.*, *15*, 43–75.

Willis, J. K. (2010), Can in situ floats and satellite altimeters detect long-term changes in Atlantic Ocean overturning?, *Geophys. Res. Lett.*, *37*, L06602, doi:10.1029/2010GL042372.

Xu, X., E. P. Chassignet, W. E. Johns, J. Schmitz Jr., and E. J. Metzger (2014), Intraseasonal to interannual variability of the Atlantic meridional overturning circulation from eddy-resolving simulations and observations, *J. Geophys. Res. Oceans*, *119*, 5140–5159, doi:10.1002/2014JC009994.

Yang, J. (1999), A linkage for decadal climate variations in Labrador Sea and tropical Atlantic Ocean, *Geophys. Res. Lett.*, *26*, 1023−1026.

Yang, J., and L. Pratt (2013), On the effective capacity of the dense-water reservoir for the Nordic Seas overflow: Some effects of topography and wind stress, *J. Phys. Oceanogr.*, *43*, 418–431.

Yang, J., and L. Pratt (2014), Some dynamical constraints on upstream pathways of the Denmark strait overflow, *J. Phys. Oceanogr.*, *44*, 3033–3053, doi:10.1175/JPO-D-13-0227.1.

Yu, L., and X. Jin (2010), Satellite-based global ocean vector wind analysis by the Objectively Analyzed Air-sea Flux (OAFlux) Project: Establishing consistent vector wind time series from July 1987 onward through synergizing microwave radiometers and scatterometers, *Tech. Rep. OA-2010-01*, WHOI OAFlux, Woods Hole Oceanographic Institution, Woods Hole, Mass.

Yu, L., J. J. O'Brien, and J. Yang (1991), On the remote forcing of the circulation in the Bay of Bengal, *J. Geophys. Res.*, *96*, 20,449–20,454.

Zhang, R. (2010), Latitudinal dependence of Atlantic meridional overturning circulation (AMOC) variations, *Geophys. Res. Lett.*, *37*, L16703, doi:10.1029/2010GL044474.

Zhao J., and W. Johns (2014), Wind-driven seasonal cycle of the Atlantic Meridional Overturning Circulation, *J. Phys. Oceanogr.*, *44*, 1541–1562, doi:10.1175/JPO-D-13-0144.1.